scientific reports

Check for updates

OPEN

Karst-bauxite formation during the Great Oxidation Event indicated by dating of authigenic rutile and its thorium content

Alexandre Raphael Cabral[1,2] & Armin Zeh[3]✉

Aluminium (Al)-rich palaeosols—i.e., palaeobauxite deposits—should have formed in karst depressions in carbonate sequences as a result of acidic solutions from oxidative weathering of sulfide minerals during the Great Oxidation Event (GOE), but no GOE-related karst-palaeobauxite deposits have so far been recorded. Here, we report results of in situ uranium–lead (U–Pb) dating of detrital zircon and spatially associated rutile from a metamorphosed Al-rich rock within a dolomite sequence in the Quadrilátero Ferrífero (QF) of Minas Gerais, Brazil, known as the Gandarela Formation. Rutile grains are highly enriched in thorium (Th = 3–46 ppm; Th/U ratio = 0.3–3.7) and yielded an isochron, lower-intercept age of ca. 2.12 Ga, which coincides with the final phase of the GOE—i.e., the Lomagundi event. The rutile age represents either authigenic growth of TiO_2 enriched in Th, U and Pb during bauxite formation, or subsequent rutile crystallisation during metamorphic overprint. Both cases require an authigenic origin for the rutile. Its high Th contents can be used as a palaeoenvironmental indicator for decreased soil pH during the GOE. Our results also have implications for iron (Fe)-ore genesis in the QF. This study demonstrates that in situ U–Th–Pb-isotope analyses of rutile can place tight constraints on the age and nature of palaeosols.

Rutile is a common accessory mineral of detrital origin in sedimentary and metasedimentary rocks. Detrital rutile has characteristically low contents of Th, generally less than 0.5 ppm Th[1]. The detrital nature of rutile reflects the very low solubility of rutile in H_2O[2], which in turn explains much of the Ti content as detrital rutile in residual products of deep weathering, such as bauxite deposits. Titanium has been demonstrated to be immobile in bauxite deposits, despite the formation of authigenic TiO_2 as anatase during bauxitisation[3].

Bauxitisation requires the removal of Fe from soils as Fe^{+2}, at low Eh conditions that are compatible with pre-2.4-Ga levels of atmospheric oxygen, before the GOE[4], recently redefined as the 'Great Oxidation Episode'[5]. While bauxitisation is possible under non-oxidative weathering, some Archaean examples of which have been recorded as metamorphosed rocks rich in Al[6], the formation of authigenic anatase in bauxitic profiles implies oxidative weathering of ilmenite ($FeTiO_3$), a major detrital source of Ti in present-day soils[7]. Authigenic anatase, as observed in present-day soils, should also have existed in palaeosols, where it is expected to be subsequently converted to rutile during prograde metamorphism[8]. Authigenic rutile has nonetheless gone unrecognised in metamorphosed bauxitic palaeosols.

Bauxitic palaeosols formed in karst depressions have not been documented during the GOE[6]. The apparent absence of karst bauxite is at odds with the GOE oxidative weathering, whereby the oxidation of sulfide minerals would have generated acidic terrestrial waters[9]. The latter would have produced karst depressions in carbonate sequences, where karst bauxites could have developed with relative Ti enrichment due to the formation of authigenic TiO_2. Here, we describe for the first time the occurrence of authigenic TiO_2 as rutile with high contents of Th in a metamorphosed karst bauxite from the Gandarela Formation of the QF. We demonstrate that authigenic rutile can be recognised by conventional reflected-light microscopy, and used as a timepiece of oxidative weathering during the GOE by applying in situ LA–ICP–SF–MS (laser ablation–inductively coupled plasma–sector field–mass spectrometry) for U–Th–Pb isotopes. We further indicate implications for the Fe-ore genesis in the QF of Minas Gerais, a world-class Fe-ore district in Brazil.

[1]Centro de Pesquisas Professor Manoel Teixeira da Costa (CPMTC), Instituto de Geociências, Universidade Federal de Minas Gerais (UFMG), Belo Horizonte, Brazil. [2]Centro de Desenvolvimento da Tecnologia Nuclear (CDTN), Belo Horizonte, Brazil. [3]Karlsruher Institut für Technologie (KIT), Campus Süd, Institut für Angewandte Geowissenschaften, Mineralogie und Petrologie, Karlsruhe, Germany. ✉email: armin.zeh@kit.edu

Study area and geological setting

The study area is a decommissioned dolomite quarry on the outskirts of Belo Horizonte (Fig. 1). The quarry, known as Acaba Mundo, exposes dolomitic rocks of the Gandarela Formation, below which is an itabirite sequence, the Cauê Itabirite of Dorr[10], likely deposited at 2.65 Ga[11]. Itabirite is a metamorphosed rock of alternating bands rich in either hematite or magnetite, and bands rich in gangue minerals, mostly quartz. The Cauê Itabirite and the Gandarela Formation, which lies with gradational contact on the former, comprise the Itabira Group of Dorr[10], or the Itabira iron formation of Harder and Chamberlin[12]. The Cauê Itabirite forms ridges that host Fe-ore deposits in the QF. One of such ridges is Serra do Curral, on the southern flank of which is Águas Claras, an itabirite-hosted world-class Fe-ore deposit[13]. In its vicinity, on the northern flank of the ridge, is the Acaba Mundo dolomite quarry.

The quarry dolomite rocks are delimited to the north by predominantly clastic rocks of the Piracicaba Group, which disconformably overlies the Itabira Group. The disconformable contact between the two groups is an erosional surface[10], the age of which has been constrained at 2141 ± 6 Ma by U–Pb dating of zircon grains from a deeply weathered sequence of pillow lavas[14]. This Palaeoproterozoic age is interpreted as the subaqueous volcanism that covered the erosional unconformity between the Itabira and the Piracicaba groups. The subaqueous volcanism occurred either shortly before or at the onset of the final phase of the Transamazonian orogeny, marked by gneiss-dome emplacement at 2095 ± 65 Ma[15]. Another orogenic event, the Brasiliano orogeny, was superimposed between 0.62 and 0.50 Ga, this time span being determined in the south-eastern QF[16].

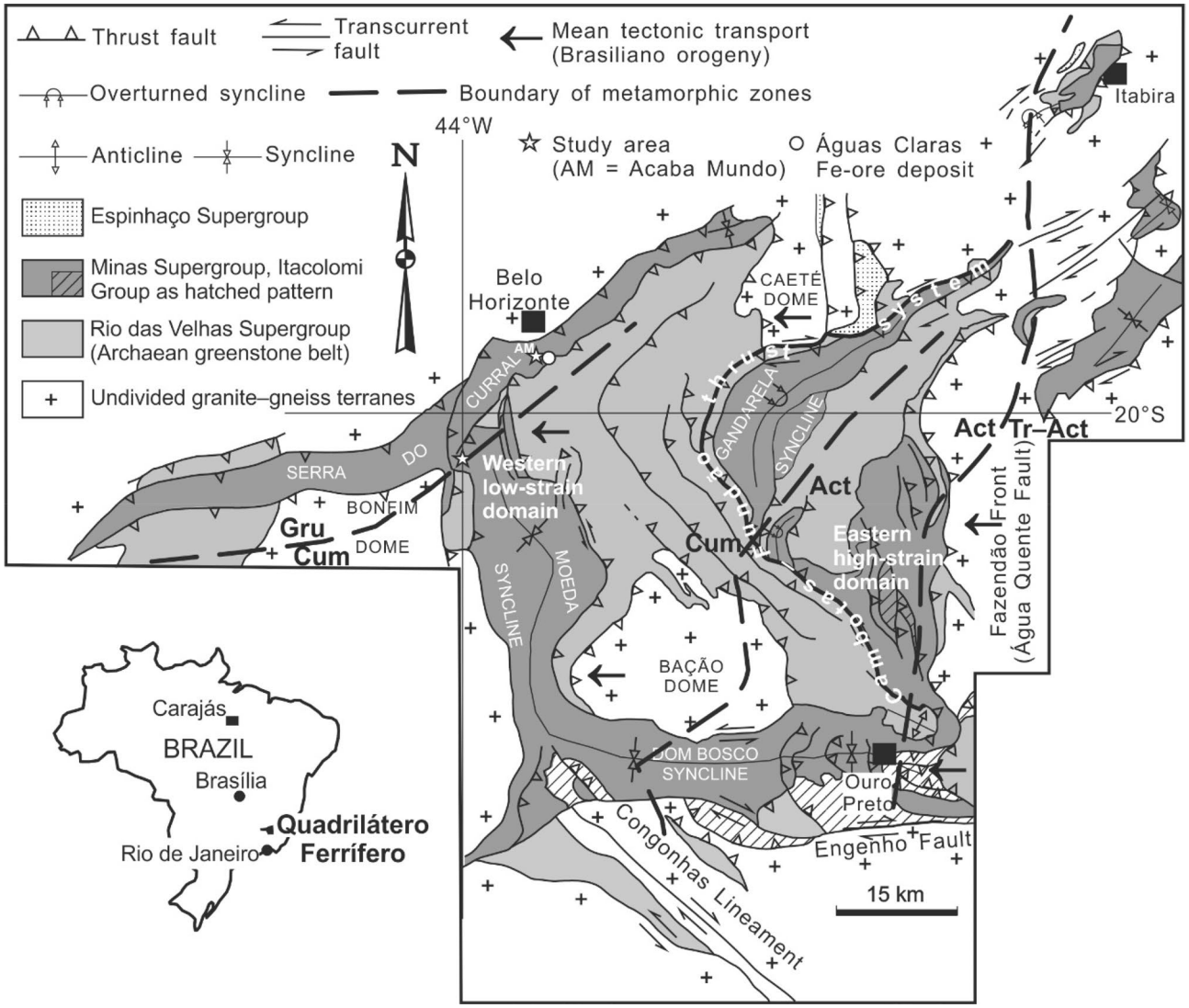

Figure 1. Location of the study area (Acaba Mundo) in the geological context of the Quadrilátero Ferrífero of Minas Gerais. The map is adapted from that presented in Rosière et al.[33], following the work of Dorr[10] and Harder and Chamberlin[12]. Metamorphic zones, based on the distribution of amphibole minerals in itabirite[42], are as follows: *Gru* grunerite, *Cum* cummingtonite, *Act* actinolite, *Tr–Act* tremolite–actinolite.

Sample material

The sample material is a dolomite-hosted body of non-foliated metamorphic rock. It has cm-long laths of a kyanite-like mineral. The mineral is extensively altered to a soft, fine-grained mineral assemblage in shades of light green to grey. The rock was sampled from the dump of an exploratory adit that was driven into the quarry dolomite. The excavated material from the adit was too aluminous for dolomite mining.

Results

The aluminous rock within the dolomite sequence of the Gandarela Formation has pyrophyllite, diaspore, muscovite and kyanite as the main mineral components (Supplementary Information Fig. S1 and Table S1). Pyrophyllite and diaspore occur as overprints on kyanite (Fig. 2). Rutile, a widespread accessory mineral in the rock (Fig. 3a,b), exhibits its distinctive internal reflections, abundant and very bright[17], as well as its characteristic geniculated twin (Fig. 3c). This elbow twin may form elongated protrusions, reaching about 0.5 mm in length (Fig. 3d). Raman spectra confirmed the reflected-light identification of rutile (Fig. 4). Another omnipresent accessory mineral is zircon (Fig. 3a,b), which is typically euhedral to round and shows no outgrowths.

The thin section investigated has a total of 20 zircon grains that could be measured by LA–ICP–SF–MS, some of them twice (Supplementary Information Table S2). Most analyses yielded discordant U–Pb ages, but seven grains returned concordant ages between ca. 3000 and ca. 2670 Ma (Fig. 5a). The youngest zircon has an age of 2666 ± 23 Ma. Measurements of 30 rutile grains gave variable $^{238}U/^{206}Pb$ ratios, with 28 analyses defining an isochrone with a lower-intercept $^{206}Pb/^{238}U$ age of 2124 ± 100 Ma (Fig. 5b; Supplementary Information Table S3). All grains show high Th contents (3–46 ppm) and elevated ratios of Th/U (0.33–3.75) and Pb/U (2–16).

Discussion

Protolith nature, detrital zircon versus authigenic rutile and the GOE. The unusually high whole-rock content of Al, mineralogically represented by kyanite that was altered to pyrophyllite, diaspore and muscovite, and the paucity of quartz and Fe-rich minerals indicate that Al was residually enriched in the protolith. Residual Al enrichment needs to be reconciled with Fe removal within the dolomite sequence of the Gandarela Formation. A likely reconciliation scenario is bauxitisation during karst weathering[3]. The karst-bauxite scenario is corroborated by the restricted occurrence of Al-rich minerals in pockets within the dolomite, and the detrital nature of zircon grains with a wide range of concordant U–Pb ages, between ca. 3000 and ca. 2660 Ma. These data imply that: (1) Archaean granite-gneiss basement rocks provided detritus to karst depressions; and (2) part of the Gandarela dolomite sequence was exposed to karst weathering and subsequent bauxitisation.

Bauxitisation under oxidative weathering is expected to form authigenic TiO_2, which is a residual product of ilmenite oxidation and progressive Fe removal[7,18]. Coarsening of authigenic TiO_2 as nanocrystalline anatase particles takes place at higher temperatures and involves twinning and rutile growth, as modelled from kinetic experiments[19]. Twinning and rutile growth during prograde metamorphism would then be expressed in the widespread occurrence of coarse-grained twinned rutile in the metamorphosed aluminous rock (Fig. 3), interpreted to have been a karst-bauxite deposit. The rutile age of 2124 ± 100 Ma reflects the timing of either authigenic TiO_2 crystallisation during karst-bauxite formation, or its subsequent metamorphic overprint.

The authigenic nature of the rutile grains can further be examined considering their high Th contents (3–46 ppm), resulting in elevated Th/U ratios (up to 3.7), far higher than those obtained from detrital rutile grains supplied from magmatic or metamorphic rocks (mostly < 0.003)[20]. The very low Th content results from the much larger size of Th^{4+} compared to Ti^{4+}, preventing its uptake during rutile growth. Nonetheless, diagenetically grown rutile in sandstone is reported to contain up to 35 ppm Th and high Th/U up to 8.75[21]. Such high Th contents

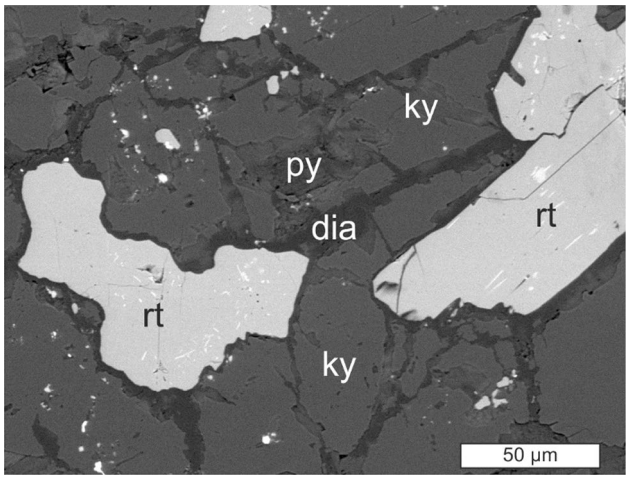

Figure 2. Backscattered-electron (BSE) image of an Al-rich rock. Pyrophyllite (py) and diaspore (dia) occur as overprint on kyanite (ky), with which rutile (rt) is spatially associated. Some rutile grains have lamellae and patches of a Cr–Fe-oxide mineral (white).

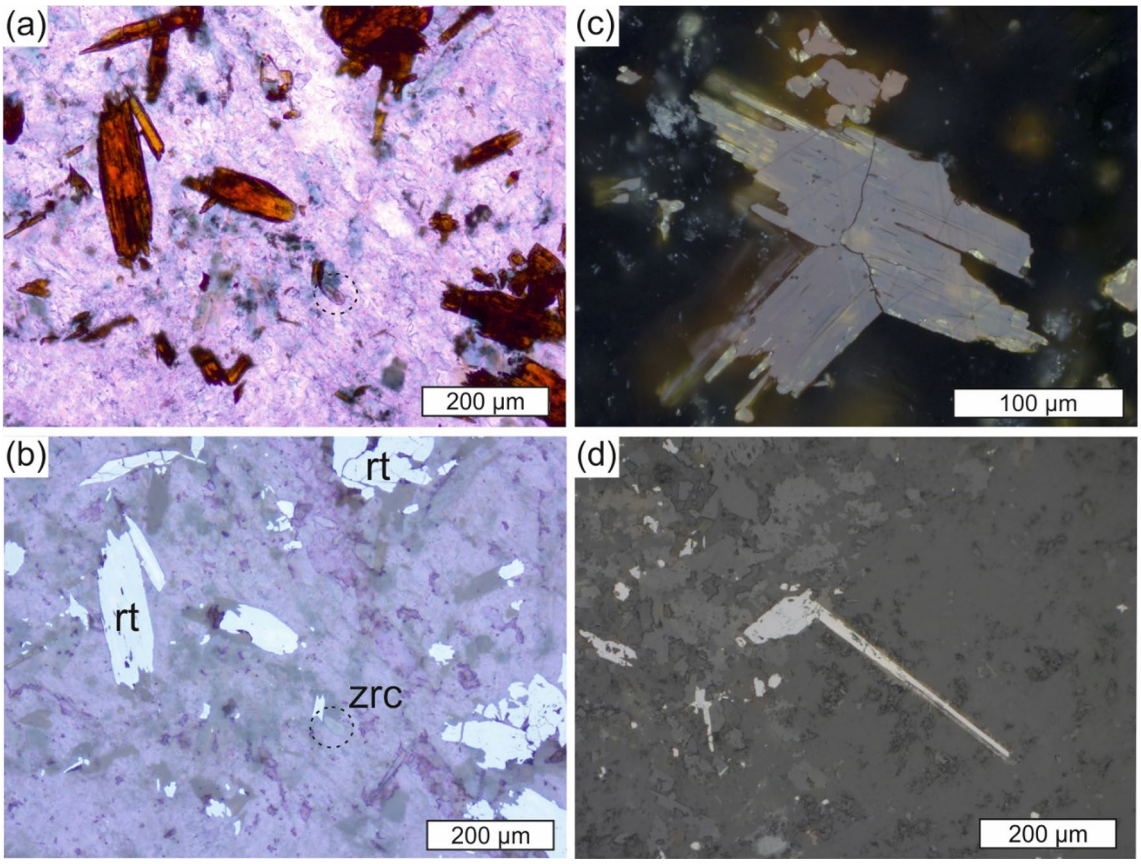

Figure 3. Photomicrographs of rutile in a kyanite–muscovite–diaspore–pyrophyllite rock. (**a**) Rutile grains show brownish-red colour in plane-parallel transmitted light. (**b**) The same rutile (rt) grains depicted in a appear grey in reflected light (air). Dashed circles in a and b denote a zircon (zrc) grain. (**c**) Twinned rutile (centre, reflected light, oil immersion). (**d**) Rutile and its protrusion stemming from a twinned contact (centre, reflected light, air).

and Th/U ratios can only be achieved by a mechanism of successive crystallisation of amorphous to poorly crystalline TiO_2 or aggregates of nanocrystalline TiO_2, leading to Th uptake into interstitial positions[22,23], in line with Th immobility during oxidative weathering[3]. Enhanced Th uptake is known from karst-bauxite anatase[23], and from authigenic rutile in low-grade sandstones of the Moeda Formation[22], underlying the Itabira Group.

Authigenic grains of rutile from the Moeda Formation yielded concordant U–Pb ages between 2245 and 2110 Ma, interpreted to date the timing of fluid–rock interaction during the Transamazonian orogeny[22]. The ages overlap with the lower-intercept age of 2124 ± 100 Ma obtained from the authigenic rutile investigated here (thereafter referred to as the bauxite rutile), but are ca. 500 Myr younger than the age of the youngest detrital zircon (2666 ± 23 Ma) in the karst bauxite, defining the maximum depositional age. The bauxite-rutile age also overlaps with an age of 2141 ± 6 Ma for the subaqueous volcanism that covers the erosional unconformity between the Itabira and the Piracicaba groups[14]. Furthermore, it is within error identical to an age of 2095 ± 65 Ma suggested to date the thermal overprint during the Transamazonian gneiss-dome emplacement in the QF[15]. However, it is significantly older than an age of 499 ± 3 Ma estimated for metamorphic rutile in the Sítio Largo amphibolite[24], recording the timing of the structural-metamorphic overprint during the Brasiliano orogeny.

In combination, stratigraphical relationships and geochronological data indicate that karstification and bauxitisation of karst-filling clastic sediments took place within the GOE, specifically at its final stage, the Lomagundi event (see below). The erosional unconformity between the Itabira and the Piracicaba groups, dated at 2.14 Ga[14], constrains the minimum age for the uplift of the Gandarela dolomite rocks and their exposure to karst weathering, during the gneiss-dome emplacement in the QF[15], immediately followed by metamorphism.

Titanium and Th mobility during the GOE. The bauxite rutile of Fig. 3d has such a long twin branch that requires input of mobile Ti. At least local mobility of Ti has been recognised in soils and sediments[25,26]. In such environments, Ti can be mobilised in the presence of organic acids. A crucial point is that metal complexing by organic ligands is mediated by highly oxidised compounds that resemble humic substances[27]. The Ti input to form the elongated protrusion of Fig. 3d is consistent with a soil where pyrite oxidation led to decreased soil pH, which increased phosphate loss and produced relative Ti enrichment, as observed in palaeosols developed during the GOE, in particular during the Lomagundi event at ca. 2.22–2.06 Ga[28]. In this regard, the high contents of common Pb determined in the bauxite rutile (Supplementary Information Table S3) could have been derived

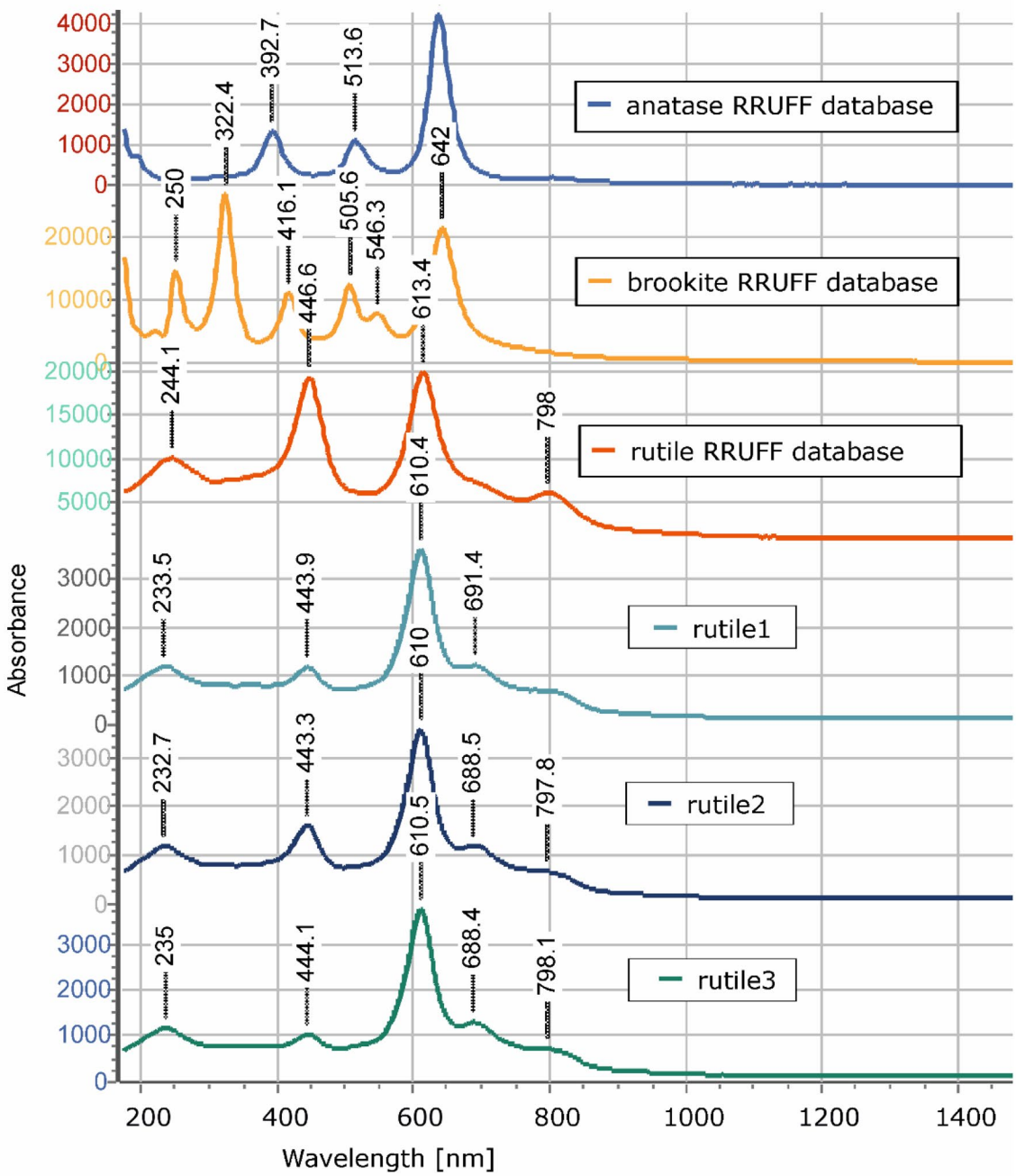

Figure 4. Raman spectra of three rutile grains, rutile 1, 2 and 3, which occur in the Al-rich rock of Figs. 2 and 3, in comparison with Raman spectra of TiO_2 polymorphs—i.e., anatase, brookite and rutile.

from aqueous solutions containing Pb from oxidised sulfide minerals. Interestingly, dissolved Pb^{+2} promotes rutile aggregation at reduced pH[29].

Importantly, reduced pH leads to increased solubilities of Th in such a manner that the concentration of soluble Th increases by seven orders of magnitude from pH 6 to pH 4 at temperatures between 18 and 25 °C[30]. Therefore, high contents of Th (> 1 ppm) in authigenic rutile might be an indicator of decreased soil pH, possibly involving organic acids, during the GOE. It should be noted, however, that Th solubilities also increase in alkaline $CaCl_2$ solutions by six orders of magnitude from pH 10 to pH 12 at temperatures between 17 and 25 °C[31].

Bauxitisation and Fe-ore genesis. An upgrade in the Fe content of itabirite to form high-grade orebodies of massive, hard hematite has been attributed to the metamorphic overprint of the Transamazonian orogeny, an interpretation supported by a U–Pb age of 2034 ± 11 Ma for monazite that coexists with granoblastic hematite after magnetite[32]. The Fe upgrade involved leaching of gangue minerals by hydrothermal fluids[33]. Much of the leaching of gangue minerals could have occurred in itabirite domains exposed to weathering, concomitant with the ca. 2.14-Ga bauxitisation of terrigenous material that filled karst depressions in the overlying dolomite sequence of the Gandarela Formation, as indicated by the results of this study.

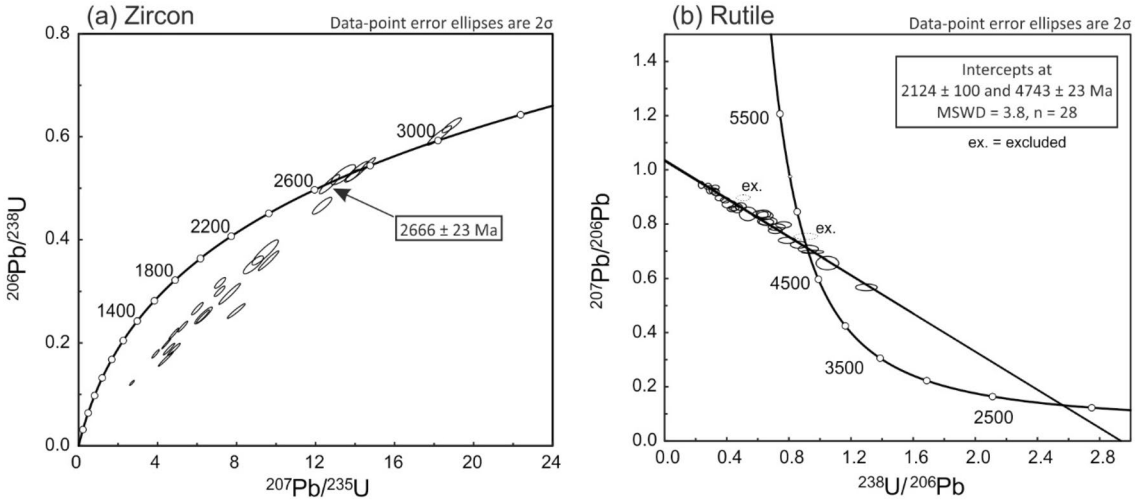

Figure 5. Concordia and Tera-Wasserburg plots for zircon (**a**) and rutile (**b**), respectively.

Conclusions

Authigenic rutile from an Al-rich rock is characterised by coarse-grained twinned crystals that are considerably younger than spatially associated grains of detrital zircon. Recognising the authigenic nature of rutile in extremely aluminous rocks enables its use as a palaeoenvironmental timepiece because: (1) authigenic TiO_2 is formed from the oxidative weathering of ilmenite, as recorded from modern weathering profiles; (2) high Th contents (> 1 ppm) attest to either acidic or alkaline soil conditions; (3) U–Pb dating of authigenic rutile and detrital zircon places age constraints. These criteria define the extremely Al-rich rock as metamorphosed karst bauxite, originally developed during the GOE over the uplifted part of the Gandarela dolomite sequence. High Th contents in authigenic rutile are consistent with decreased soil pH during the GOE.

Methods

One sample of the aluminous rock was cut for polished-thin-section preparation; an aliquot of it was milled for powder X-ray diffraction (XRD), performed using a PANalytical X'Pert Pro instrument, with a Cu*Kα* source and a proportional point detector (PW 3011/20). The instrument, housed at the Instituto de Geociências, Universidade Federal de Minas Gerais, was operated at 40 kV and 45 mA. Data collection was in Bragg–Brentano geometry from 5° to 69° (2θ), with 0.02° (2θ) steps at 0.5 s per step. All XRD data are presented in Supplementary Information Table S1 and Fig. S1.

Raman spectra were collected on three representative rutile grains using a Bruker Senterra spectrometer, coupled to an Olympus BX51 light microscope, at the Institute of Applied Geosciences, Karlsruhe Institute of Technology (KIT), Germany. A 532-nm laser, the power of which was 2 mW, with aperture of 50 µm and total time of 30 s (3 s times 10 coadditions), was focused onto specimens with a 20×-microscope lens (OLYMPUS M-PLAN 20x), resulting in a spot diameter of approximately 5 µm on the sample surface.

Measurements for U–Th–Pb isotopes in zircon and rutile were performed in situ on a polished thin section, using a 193-nm ArF Excimer laser (Analyte Exite+, Teledyne Photon Machines), coupled to a ThermoScientific Element XR instrument at the KIT. Twenty zircon grains, < 60 µm in length, were large enough for LA–ICP–SF–MS dating using a laser spot size of 20 µm. The grains are rounded and some of them show oscillatory zoning typical of magmatic zircon. Rutile, brownish-red colour in transmitted light (Fig. 3a), was analysed with a laser spot size of 50 µm on grains that were free of optically discernible inclusions and pores (Fig. 3b). Optical microscopy was complemented by scanning electron microscopy (TESCAN VEGA2 SBH with Oxford SwiftED EDS system) for locating sufficiently large, inclusion-free zircon and rutile grains.

Zircon grains of unknown age were dated together with the reference zircon material BB (primary standard), Plešovice and KA (KaapValley), using a laser spot diameter of 20 µm, a laser fluence of 2.7 J/cm^2, at 10-Hz repetition rate, RF = 1255 W, a mixed Ar–He–N_2 carrier gas consisting of Ar = 0.965 l/min, He = 0.30 cell + 0.21 cup (both l/min), and N_2 = 13 ml/min. Three pulses of pre-ablation were performed prior to each analysis of 15-s duration, following 15-s background measurement. All raw data were corrected offline for daily instrumental drift and mass offset employing an in-house MS Excel© spreadsheet programme[34,35]. We applied a common-Pb correction based on the interference- and background-corrected ^{204}Pb signal, and a model Pb composition[36]. Results of U–Pb dating of reference zircon and unknows are shown in Supplementary Information Table S2. Multiple measurements of the reference zircon BB (primary standard), Plešovice and KA (KaapValley) (secondary standards) yielded Concordia ages of 561.6 ± 3.2 Ma (MSWD = 0.1, probability = 0.98, n = 10), 338.9 ± 1.4 Ma (MSWD = 0.1, probability = 0.99, n = 10), and 3225.8 ± 7.9 Ma (MSWD = 5.3, probability = 0.02, n = 10), respectively, in agreement with published TIMS ages[37–39].

Rutile grains of unknown age were dated using the same instrument and setup conditions that are described above. Rutile R10[40] was employed for matrix-matched primary standard to correct for instrumental ^{206}Pb/^{238}U mass offset. Multiple analyses of the reference rutile (R10) gave a Concordia age of 1089.8 ± 7.4 Ma (MSWD = 0.21, probability = 0.65, n = 10), in agreement with published TIMS values[40]. Results of U–Th–Pb-isotope analyses of

reference rutile and unknowns are shown in Supplementary Information Table S3. Concordia and Tera-Wasserburg diagrams were plotted by means of the software ISOPLOT 4.15[41]. Operation conditions are detailed in Supplementary Information Table S4.

Data availability

All raw data used for this manuscript are included within the Supplementary Information files.

Received: 18 February 2023; Accepted: 20 May 2023
Published online: 27 May 2023

References

1. Zack, T. & Kooijman, E. Petrology and geochronology of rutile. *Rev. Mineral. Geochem.* **83**, 443–467 (2017).
2. Tropper, P. & Manning, C. E. Very low solubility of rutile in H_2O at high pressure and temperature, and its implications for Ti mobility in subduction zones. *Am. Mineral.* **90**, 502–505 (2005).
3. MacLean, W. H., Bonavia, F. F. & Sanna, G. Argillite debris converted to bauxite during karst weathering: Evidence from immobile element geochemistry at the Olmedo Deposit, Sardinia. *Miner. Depos.* **32**, 607–616 (1997).
4. Holland, H. D. Sedimentary mineral deposits and the evolution of Earth's near-surface environments. *Econ. Geol.* **100**, 1489–1509 (2005).
5. Poulton, S. W. *et al.* A 200-million-year delay in permanent atmospheric oxygenation. *Nature* **592**, 232–236 (2021).
6. Retallack, G. J. Lateritization and bauxitization events. *Econ. Geol.* **105**, 655–667 (2010).
7. Anand, R. R. & Gilkes, R. J. Weathering of ilmenite in a lateritic pallid zone. *Clays Clay Miner.* **32**, 363–374 (1984).
8. Banfield, J. F., Bischoff, B. L. & Anderson, M. A. TiO_2 accessory minerals: Coarsening, and transformation kinetics in pure and doped synthetic nanocrystalline materials. *Chem. Geol.* **110**, 211–231 (1993).
9. Konhauser, K. O. *et al.* Aerobic bacterial pyrite oxidation and acid rock drainage during the Great Oxidation Event. *Nature* **478**, 369–373 (2011).
10. Dorr, J. V. N. II. Physiographic, stratigraphic and structural development of the Quadrilátero Ferrífero, Minas Gerais, Brazil. *U.S. Geol. Surv. Prof. Pap.* **641**, 1–110 (1969).
11. Cabral, A. R. *et al.* Dating the Itabira iron formation, Quadrilátero Ferrífero of Minas Gerais, Brazil, at 2.65 Ga: Depositional U–Pb age of zircon from a metavolcanic layer. *Precambrian Res.* **204–205**, 40–45 (2012).
12. Harder, E. C. & Chamberlin, R. T. The geology of central Minas Geraes, Brazil. *J. Geol.* **23**, 341–378, 385–424 (1915).
13. Spier, C. A., de Oliveira, S. M. B. & Rosière, C. A. Geology and geochemistry of the Águas Claras and Pico Iron Mines, Quadrilátero Ferrífero, Minas Gerais, Brazil. *Miner. Depos.* **38**, 751–774 (2003).
14. Cabral, A. R. *et al.* Unconformity-covering pillow lava dated at 2.14 Ga: Challenging the "stable-shelf" minas supergroup of the Quadrilátero Ferrífero, Minas Gerais, Brazil. *Geol. J.* **57**, 2046–2057 (2022).
15. Marshak, S., Tinkham, D., Alkmim, F., Brueckner, H. & Bornhorst, T. Dome-and-keel provinces formed during Paleoproterozoic orogenic collapse—Core complexes, diapirs, or neither?: Examples from the Quadrilátero Ferrífero and the Penokean orogen. *Geology* **25**, 415–418 (1997).
16. Cabral, A. R., Zeh, A., Tupinambá, M. & Pimenta, J. First evidence for Neoproterozoic magmatism in the Quadrilátero Ferrífero of Minas Gerais, Brazil, and geotectonic implications. *J. S. Am. Earth Sci.* **104**, 102844 (2020).
17. Ramdohr, P. *Die Erzmineralien und ihre Verwachsungen* (Akademie-Verlag, 1960).
18. Teufer, G. & Temple, A. K. Pseudorutile—A new mineral intermediate between ilmenite and rutile in the natural alteration of ilmenite. *Nature* **211**, 179–181 (1966).
19. Zhang, H. & Banfield, J. F. New kinetic model for the nanocrystalline anatase-to-rutile transformation revealing rate dependence on number of particles. *Am. Mineral.* **84**, 528–535 (1999).
20. Zack, T. *et al.* In situ U–Pb rutile dating by LA–ICP–MS: ^{208}Pb correction and prospects for geological applications. *Contrib. Mineral. Petrol.* **162**, 515–530 (2011).
21. Dunkl, I. & von Eynatten, H. Anchizonal-hydrothermal growth and (U–Th)/He dating of rutile crystals in the sediments of Hawasina window, Oman. *Geochim. Cosmochim. Acta* **73**, A314 (2009).
22. Zeh, A., Cabral, A. R., Koglin, N. & Decker, M. Rutile alteration and authigenic growth in metasandstones of the Moeda Formation, Minas Gerais, Brazil—A result of Transamazonian fluid–rock interaction. *Chem. Geol.* **483**, 397–409 (2018).
23. Gamaletsos, P. *et al.* Thorium partitioning in Greek industrial bauxite investigated by synchrotron radiation and laser-ablation techniques. *Nucl. Instrum. Methods Phys. Res. B* **269**, 3067–3073 (2011).
24. Cabral, A. R. & Zeh, A. Celebrating the centenary of "The Geology of Central Minas Gerais, Brazil": An insight from the Sítio Largo amphibolite. *J. Geol.* **123**, 337–354 (2015).
25. Milnes, A. R. & Fitzpatrick, R. W. Titanium and zirconium minerals in *Minerals in Soil Environments* (2nd edition), 1131–1205 (Soil Science Society of America, Book Series 1, 1989).
26. Imperial, A., Pe-Piper, G., Piper, D. J. W. & Clyburne, J. The use of titania polymorphs as indicators of mesodiagenesis during hydrocarbon charge. *Mar. Pet. Geol.* **149**, 106075 (2023).
27. Reuter, J. H. & Perdue, E. M. Importance of heavy metal–organic matter interactions in natural waters. *Geochim. Cosmochim. Acta* **41**, 325–334 (1977).
28. Bekker, A. & Holland, H. D. Oxygen overshoot and recovery during the early Paleoproterozoic. *Earth Planet. Sci. Lett.* **317–318**, 295–304 (2012).
29. Ledingham, G. J., Pan, W., Giammar, D. E. & Catalano, J. G. Exchange of adsorbed Pb(II) at the rutile surface: rates and mechanisms. *Environ. Sci. Technol.* **56**, 12169–12178 (2022).
30. Neck, V. *et al.* Solubility of amorphous Th(IV) hydroxide—Application of LIBD to determine the solubility product and EXAFS for aqueous speciation. *Radiochim. Acta* **90**, 485–494 (2002).
31. Brendebach, B., Altmaier, M., Rothe, J., Neck, V. & Denecke, M. A. EXAFS study of aqueous Zr^{IV} and Th^{IV} Complexes in alkaline $CaCl_2$ solutions: $Ca_3[Zr(OH)_6]^{4+}$ and $Ca_4[Th(OH)_8]^{4+}$. *Inorg. Chem.* **46**, 6804–6810 (2007).
32. Sanglard, J. C. D., Rosière, C. A., Santos, J. O. S., McNaughton, N. J. & Fletcher, I. R. A estrutura do segmento oeste da Serra do Curral, Quadrilátero Ferrífero, e o controle tectônico das acumulações compactas de alto teor em Fe. *Geol. USP Sér. Cient.* **14**, 81–95 (2014).
33. Rosière, C. A., Spier, C. A., Rios, F. J. & Suckau, V. E. The itabirites of the Quadrilátero Ferrífero and related high-grade iron ore deposits: An overview. *Rev. Econ. Geol.* **15**, 223–254 (2008).
34. Gerdes, A. & Zeh, A. Combined U–Pb and Hf isotope LA–(MC–)ICP–MS analyses of detrital zircons: Comparison with SHRIMP and new constraints for the provenance and age of an Armorican metasediment in Central Germany. *Earth Planet. Sci. Lett.* **249**, 47–61 (2006).

35. Gerdes, A. & Zeh, A. Zircon formation versus zircon alteration—New insights from combined U–Pb and Lu–Hf in-situ LA–ICP–MS analyses, and consequences for the interpretation of Archean zircon from the Central Zone of the Limpopo Belt. *Chem. Geol.* **261**, 230–243 (2009).
36. Stacey, J. S. & Kramers, J. D. Approximation of terrestrial lead isotope evolution by a two-stage model. *Earth Planet. Sci. Lett.* **26**, 207–221 (1975).
37. Santos, M. M. *et al.* A new appraisal of Sri Lankan BB zircon as a reference material for LA–ICP–MS U–Pb geochronology and Lu–Hf isotope tracing. *Geostand. Geoanal. Res.* **41**, 335–358 (2017).
38. Schoene, B., Crowley, J. L., Condon, D. J., Schmitz, M. D. & Bowring, S. A. Reassessing the uranium decay constants for geochronology using ID-TIMS U–Pb data. *Geochim. Cosmochim. Acta* **70**, 426–445 (2006).
39. Sláma, J. *et al.* Plešovice zircon—A new natural reference material for U–Pb and Hf isotopic microanalysis. *Chem. Geol.* **249**, 1–35 (2008).
40. Luvizotto, G. L. *et al.* Rutile crystals as potential trace element and isotope mineral standards for microanalysis. *Chem. Geol.* **261**, 346–369 (2009).
41. Ludwig, K. R. *User's manual for Isoplot 3.75: A geochronological toolkit for Microsoft Excel* (Berkeley Geochronology Center Special Publication, 2012).
42. Pires, F. R. M. Textural and mineralogical variations during metamorphism of the Proterozoic Itabira iron formation in the Quadrilátero Ferrífero, Minas Gerais, Brazil. *An. Acad. Bras. Ciê.* **67**, 77–105 (1995).

Acknowledgements

Mr. Ulf Hemmerling and Dr. Stephanie Lohmeier (Technische Universität Clausthal, Germany) are thanked for thin-section preparation. A.R.C. gratefully acknowledges Mr. Lucas de Pádua Ribeiro for having taken part in the fieldwork, and Dr. Igor Santana for XRD analysis. A.Z. thanks Dr. Kirsten Drüppel (KIT) for help with Raman spectrometry. Editorial handling by Dr. Greg Shellnutt and thoughtful comments by two anonymous referees are also acknowledged.

Author contributions

A.R.C. designed the research, carried out fieldwork and ore-mineral petrography; A.Z. performed U–Pb dating of zircon and rutile. Both authors wrote the manuscript.

Funding

Open Access funding enabled and organised by Projekt DEAL.

Competing interests

The authors declare no competing interests.

Additional information

Supplementary Information The online version contains supplementary material available at https://doi.org/10.1038/s41598-023-35574-x.

Correspondence and requests for materials should be addressed to A.Z.

Reprints and permissions information is available at www.nature.com/reprints.

Publisher's note Springer Nature remains neutral with regard to jurisdictional claims in published maps and institutional affiliations.